Frontiers in Bioscience Landmark

Front. Biosci. (Landmark Ed) **2024**; 29(1): 27
https://doi.org/10.31083/j.fbl2901027

Original Research

KLF8 Promotes the Survival of Lung Adenocarcinoma During Nutrient Deprivation by Regulating the Pentose Phosphate Pathway through SIRT2

Qiaohong Bai[1,†], Wenfang Jin[1,†], Futao Chen[2], Jiang Zhu[2], Lifeng Cao[2], Yang Yang[2], Fukuan Zhong[2], Li Li[3,*]

[1]Department of Respiratory, The Second Hospital of Nanjing, Nanjing University of Chinese Medicine, 210000 Nanjing, Jiangsu, China
[2]Department of Respiratory, The Second Hospital of Lianyungang, 222000 Lianyungang, Jiangsu, China
[3]Department of Respiratory, Nanjing Chest Hospital, Affiliated Nanjing Brain Hospital, Nanjing Medical University, 210000 Nanjing, Jiangsu, China
*Correspondence: lilizby@163.com (Li Li)
[†]These authors contributed equally.

Academic Editors: Fu Wang and Graham Pawelec
Submitted: 29 May 2023 Revised: 8 September 2023 Accepted: 7 October 2023 Published: 18 January 2024

Abstract

Background: The pentose phosphate pathway (PPP) is a critical metabolic pathway that generates NADPH and ribose-5-phosphate for nucleotide biosynthesis and redox homeostasis. In this study, we investigated a potential regulatory role for Krüppel-like factor 8 (KLF8) in the control of PPP in lung adenocarcinoma (LUAD) cells. **Methods**: Based on a comprehensive set of experimental approaches, including cell culture, molecular techniques, and functional assays, we revealed a novel mechanism by which KLF8 promotes the activation of glucose-6-phosphate dehydrogenase (G6PD), a component enzyme in the PPP. **Results**: Our findings demonstrate that KLF8 inhibits the acetylation of G6PD, leading to its increased enzymatic activity. Additionally, we observed that KLF8 activates the transcription of SIRT2, which has been implicated in regulating G6PD acetylation. These results highlight the interplay between KLF8, G6PD, and protein acetylation in the regulation of PPP in LUAD. **Conclusions**: Understanding the intricate molecular mechanisms underlying the metabolic reprogramming driven by KLF8 in lung cancer provides valuable insights into potential therapeutic strategies targeting the PPP. This study emphasizes the significance of KLF8 as a key modulator of metabolic pathways and indicates the potential of targeting the KLF8-G6PD axis for lung cancer treatment.

Keywords: pentose phosphate pathway; nutrient deprivation; KLF8; tumor metabolism

1. Introduction

Lung adenocarcinoma (LUAD) is a subtype of non-small cell lung cancer (NSCLC) and is a prevalent and aggressive malignancy characterized by distinct histological features and high mortality rates [1]. LUAD is known to undergo metabolic reprogramming to enable rapid proliferation and growth, even under conditions of nutrient deprivation [2]. However, during the early stages of tumor development, delays in neoangiogenesis can lead to poor nutrient supply. Such conditions necessitate the activation/deactivation of signaling pathways to adapt to the harsh environment, as well as meeting metabolic demands while maintaining redox balance [3].

The pentose phosphate pathway (PPP) is a metabolic pathway that runs parallel to glycolysis and is an important mechanism for cells to generate reducing power and nucleotides necessary for numerous biosynthetic activities [4]. PPP can bypass glycolysis and provide NADPH, which is crucial for scavenging reactive oxygen species (ROS) and maintaining redox balance [5,6]. During nutrient deprivation, metabolic stress is induced in cancer cells, glucose uptake is reduced, and glycolysis and the PPP is impaired. These conditions lead to decreased ATP production, elevated ROS production and oxidative stress, and subsequent redox imbalance and cell death [7–9]. The activation of PPP under serum starvation benefits cancer cell survival by reducing ROS generation and enhancing nucleotide and lipid synthesis [10].

Glucose-6-phosphate dehydrogenase (G6PD) is a key rate-limiting enzyme in the PPP, and is activated under oxidative stress induced lipopolysaccharides to maintain redox balance by converting glucose-6-phosphate (G6P) to 6-phosphoglucono-δ-lactone in the presence of $NADP^+$, thus generating NADPH in its catalytic cycle [11]. Notably, glucose starvation can induce oxidative stress in cancer progression [12]. In a previous study, it was found that the G6PD expression was not significantly changed by TSC2 silencing under glucose-restricted, normoxic conditions [13]. However, it has also been demonstrated that G6PD is associated with cell survival, and serum deprivation as a cell death stimulator can result in both reduced G6PD activity and increased ROS levels [14].

Krüppel-like factor 8 (KLF8) is a transcription factor with zinc finger domains that regulates various biological processes, including tumor proliferation, epithelial-

mesenchymal transition, metastasis, and drug resistance [15,16]. Previous research has indicated that KLF8 is upregulated in LUAD cells under serum-starved conditions [17], and can promote lung cancer proliferation and metastasis [18]. However, the exact nature of the mechanism(s) by which KLF8 contributes to these effects remains unknown.

SIRT2, a member of the sirtuin family of deacetylases, is involved in various cellular processes and is implicated in cancer development and progression [19]. It has been shown previously that KAT9 and SIRT2 can regulate G6PD acetylation [20]. In LUAD, higher mRNA and protein levels of SIRT2 have been revealed to affect prognosis and are associated with better overall survival (OS) [21]. Nevertheless, whether SIRT2 interacts with other proteins requires further study.

Given these findings, we hypothesize that KLF8 may play a role in regulating the PPP and promoting the survival of LUAD cells under nutrient-deprived conditions. A better understanding of this mechanism may provide clues for the development of new therapeutic strategies for treating LUAD.

2. Materials and Methods

2.1 Bioinformatic Analysis

Gene Expression Omnibus (GEO) is a publicly available database that provides gene expression data for various organisms, including humans. In this study, the GEO dataset GSE62663 (https://www.ncbi.nlm.nih.gov/geo/query/acc.cgi?acc=GSE62663) was analyzed using GEO2R to examine the expression levels of KLF8 in LUAD cells under different culture conditions [22]. Gene Expression Profiling Interactive Analysis (GEPIA, http://gepia.cancer-pku.cn/) is a web-based tool that allows users to analyze gene expression data from the Cancer Genome Atlas (TCGA, http://cancergenome.nih.gov/) and the Genotype-Tissue Expression (GTEx, https://www.gtexportal.org/home/) project. In this study, GEPIA was used to assess the correlation between KLF8 and the histone acetyltransferase KAT9 and the deacetylase SIRT2 in LUAD. Human Transcription Factor Database (HumanTFDB, http://bioinfo.life.hust.edu.cn/HumanTFDB#!/) is a comprehensive database that provides information regarding transcription factors and their binding sites. In this study, the HumanTFDB website was used to predict the binding sites of KLF8 and SIRT2 within the promoter regions of their target genes.

2.2 Clinical Samples

Lung adenocarcinoma tissues (n = 30) and adjacent normal tissues (n = 30) were collected from patients with LUAD in our hospital. Samples were immediately stored at –80 °C for further analysis. The Ethics Committee of our hospital has approved this study, and all patients who participated in this study have signed a written informed consent.

2.3 Cell Culture

BEAS-2B cells (95102433, ECACC, UK) were cultured in Bronchial Epithelial Cell Growth Medium (BEGM, CC-3171, Lonza, Switzerland). A549, H1299, HCC827 and H460 cells (CCL-185; CRL-5803; CRL-2868; HTB-177, ATCC, Manassas, VA, USA) were incubated in RPMI-1640 (11875093, Gibco, Thermo Fisher Scientific, Waltham, MA, USA) with 10% fetal bovine serum (FBS, 10270-106, Gibco, Grand Island, NY, USA). Prior to experimentation, the cells were allowed to attach overnight in a humidified incubator at 37 °C with 5% CO_2. The next day, nutrient-deprived medium was added for an additional 48 h incubation, as indicated. The nutrient-deprived medium was prepared by using BEGM without the addition of FBS.

A Mycoplasma PCR Detection Kit (AAJ66117AMJ, Thermo Fisher Scientific) was used for screening for potential mycoplasma infection. Cells have been authenticated by short tandem repeat (STR) profiling, which are listed by corresponding manufacturers on their product websites.

2.4 Cell Transfection

The short hairpin RNAs (shRNAs) targeting KLF8 (sh-KLF8, 5′-CAGCACTGTTTAATGACAT-3′) and a corresponding negative (non-targeting) control (sh-NC, 5′-TTCTCCGAACGTGTCACGT-3′) were designed and synthesized into the shRNA expression vector (pGPU6/mCherry/Puro) by GenePharma Co. Ltd. (Shanghai, China). To overexpress FLF8 and G6PD, pcDNA3.1/KLF8, and pcDNA3.1/G6PD vectors were constructed and provided by the Genomeditech Shanghai Co., Ltd. (Shanghai), and empty pcDNA3.1 vector was used as the negative control. H1299 and A549 cells were seeded into 6-well plates at 3×10^5 cells/well and transfected with the above vectors or negative control vectors using Lipofectamine 3000 (Invitrogen, Waltham, MA, USA). The stably transfected cells were selected using puromycin [23].

2.5 Western Blotting

Protein extracts were prepared using Radio Immunoprecipitation Assay (RIPA) lysis buffer (Thermo Fisher Scientific) and protein concentrations measured using a Bicinchoninic acid (BCA) protein assay kit (23225, Thermo Fisher Scientific). Proteins were subsequently separated by SDS-PAGE and transfered to (polyvinylidene difluoride) PVDF membranes (IPVH00010, Millipore, Burlington, MA, USA). Following this, membranes were cultured with anti-KLF8 (1:1000, ab168527, Abcam), G6PD (1:1000, ab210702, Abcam, Cambridge, UK), anti-SIRT2 (1:1000, 12640, Cell Signaling, Danvers, MA, USA) and anti-β-actin (1:1000, AF0003, Beyotime, Shanghai, China) at 4 °C overnight. After washing the membranes, secondary antibodies (A0208, 1:1000, Beyotime) were added for a 1 h incubation at room temperature. Enhanced chemiluminescence reagent (P0018, Beyotime) and ImageJ2 software

(LOCI, University of Wisconsin, Madison, WI, USA) were used for visualization and quantification of proteins.

2.6 Immunohistochemistry

After deparaffinization and rehydration, tissue sections from LUAD patients were incubated with anti-KLF8 (1/200, ab137676, Abcam, UK) primary antibody overnight at 4 °C. This step was followed by incubation with appropriate HRP-conjugated secondary antibody (1/5000, ab97051, Abcam). The slides were visualized using DAB (3,3′-Diaminobenzidine) substrate (ab94665, Abcam) and counterstained with hematoxylin. Images were captured using a light microscope (Olympus, Tokyo, Japan).

2.7 Quantitative Real-Time Polymerase Chain Reaction

PrimeScript RT reagent kit (RR037A, TaKaRa, Beijing, China) was used for cDNA synthesis. Quantitative real-time PCR (qRT-PCR) was performed using a LightCycler 480 Real-Time PCR System (Roche Diagnostics, Rotkreuz, Switzerland) and SYBR Premix Ex Taq II (RR820A, TaKaRa). The primers used in qRT-PCR were as follows: KLF8(Forward): 5′-TATTCAAGCAGGTCACTGC-3′, KLF8(Reverse): 5′-CAGGAGTGTTGGAGAAGTC-3′; G6PD(Forward): 5′-GTGAGGACCAGATCTACCG-3′, G6PD(Reverse): 5′-TGTTGGCAAATCTCAGCAC-3′; SIRT2(Forward): 5′-AGCTGGAATCTCCACATCC-3′, SIRT2(Reverse): 5′-CCGGATGTTTCTTGAAATAGCT-3′; GAPDH(Forward): 5′-AGCCACATCGCTCAGACAC-3′, GAPDH(Reverse): 5′-GCCCAATACGACCAAATCC-3′.

2.8 Cell Counting Kit-8

Nighty-six-well plates were inoculated at 5000 cells/well. Forty-eight hours later, 10 µL of Cell counting kit-8 (CCK-8) reagent (CK04-11, Dojindo, Kyushu Island, Japan) was added to each well. After a 2 hr incubation at 37 °C, absorbance at 450 nm was recorded using a BioTek Epoch microplate reader (Agilent, Beijing, China).

2.9 Colony Formation Assay

Six-well plates were inoculated at 500 cells/well, with medium refreshed every 3 days. Paraformaldehyde (4%) was used to fix the cell monolayer for 15 min and crystal violet solution (0.1%, C0775, Sigma-Aldrich, St. Louis, MO, USA) was used to stain the colonies for 30 min. Excess stain was rinsed off with water, and the plates were air-dried. The number of visible colonies, defined as clusters of at least 50 cells, was counted manually under a light microscope (Olympus, Japan).

2.10 Flow Cytometry

After washing with pre-chilled PBS, H1299 and A549 cells (2×10^5 cells) were collected by centrifugation for 5 min at 1500 g. Then cells were then resuspended in binding buffer containing 5 µL Annexin-V-FITC and 5 µL propidium iodide (PI) and incubated for 20 min at room temperature in dark. Cell staining was analyzed using a flow cytometer (BD Biosciences, San Jose, CA, USA). With AnnexinV staining set on the horizontal axis and PI staining as the vertical axis, the apoptotic cells were quantified using CellQuest software (version 5.1, BD Biosciences).

2.11 Fluorescence Assay for ROS Measurement

To assess ROS in H1299 and A549 cells, a fluorescence assay was performed using 2′,7′-dichlorofluorescein diacetate (DCFH-DA) probe (Beyotime). Briefly, 96-well plates were inoculated with LUAD cells at 5×10^3 cells/well. Then cells were washed and treated with 10 µM DCFH-DA (D6883, Sigma-Aldrich) at 37 °C for 30 min. The fluorescence intensity of 2′,7′-dichlorofluorescein, indicative of ROS levels, was analyzed using a fluorescence microplate reader (PerkinElmer, Waltham, MA, USA).

2.12 Colorimetric Assay for NADPH/$NADP^+$ Detection

The levels of $NADP^+$/NADPH in RIPA protein extracts were assayed based on the enzymatic cycling reaction using a commercial kit (ab65349, Abcam). Briefly, co-incubation of cell lysates, reaction buffer, and NADPH cycling enzyme mix was conducted for 30 min and results were obtained using a spectrophotometer at an absorbance of 450 nm.

2.13 Measurement of Oxidative PPP Flux

Oxidative PPP flux was determined by measuring $^{14}CO_2$ release as previously indicated [24]. LUAD cells were incubated in a 6-cm dish within a 10-cm dish containing two sealed pinholes on top. Cells were exposed to 2 mL of medium containing [6-^{14}C]-glucose or [1-^{14}C]-glucose for 3 h at 37 °C. To halt the PPP flux, 0.3 mL of 50% TCA was injected through one pinhole, with 0.3 mL of hyamine hydroxide injected through the second pinhole at the same time. Following this, both dishes were sealed and incubated overnight at room temperature. Hyamine hydroxide was dissolved in 60% methanol and subsequently analyzed via scintillation counting (Beckman Coulter, LS6500 Scintillation Counter, GA, USA).

2.14 Measurement of RNA Synthesis

H1299 and A549 cells were seeded in culture plates and allowed to adhere overnight. Cells were then treated with 1 mM 5-ethynyl uridine (EU) (E10345, Thermo Fisher Scientific) for 1 h. Next, cells were harvested, and total RNA extracted using a QIAGEN RNeasy Mini Kit (74104, QIAGEN, Hilden, Germany). The EU incorporated into RNA was then labeled using an EU detection kit (C10329, Click-iT RNA Imaging Kit, Thermo Fisher Scientific). Labeled RNA was visualized using fluorescence microscopy (Leica, Wetzlar, Germany), and the intensity of the fluo-

rescence signal was quantified using ImageJ2. The fluorescence intensity directly corresponds to the level of nascently synthesized RNA in the cells.

2.15 Measurement of G6PD Protein Activity

H1299 and A549 cells were lysed and centrifuged, and the supernatant containing the protein extracts was collected. To measure G6PD activity, a G6PD assay kit (ab102529, Abcam, UK) was used. The reaction mixture, consisting of cell lysate, reaction buffer, and $NADP^+$ cycling enzyme mix, was incubated for 30 min at 37 °C. The enzymatic reaction catalyzed by G6PD results in the reduction $NADP^+$/NADPH, which was visualized by a change in absorbance. The absorbance was measured at 450 nm using a BioTek Epoch microplate reader. The rate of NADPH production, indicated by the change in absorbance over time, was used as a measure of G6PD enzyme activity.

2.16 Immunoprecipitation

Briefly, H1299 and A549 cells were lysed and precleared with protein A/G beads (sc-2003, Santa Cruz Biotechnology, Shanghai, China). Anti-G6PD antibody (ab993, Abcam) was added for incubation overnight at 4 °C. The immunocomplexes were collected with protein A/G beads and washed with lysis buffer. The beads were then eluted with 2× SDS sample buffer (1610737, Bio-Rad, Hercules, CA, USA) and the eluted proteins were analyzed via western blotting using anti-acetylated-Lysine antibody (9441, Cell Signaling) to detect the acetylation of G6PD. The signals were detected using enhanced chemiluminescence (34095, Thermo Fisher Scientific).

2.17 Dual Luciferase Activity Reporter Assay

The binding sites of KLF8 on SIRT2 promoters were predicted by the HumanTFDB website. The SIRT2 fragments containing wild-type (WT) or mutant (Mut) binding sequences were subcloned into the pGL3-basic luciferase reporter vectors to construct promoter-WT or promoter-Mut plasmids. Subsequently, H1299 and A549 cells were co-transfected with promoter-WT or promoter-Mut constructs along with sh-NC or sh-KLF8 using Lipofectamine 2000 (Thermo Fisher Scientific). After 48 h, the cells were lysed using Passive Lysis Buffer (E1941, Promega, USA). Luciferase activity was measured using a Dual-Luciferase Reporter Assay System (E1910, Promega, Madison, WI, USA). Relative Firefly luciferase activity was normalized to Renilla luciferase as the internal standard. The relative luciferase activity was calculated by comparing the promoter-WT or promoter-Mut transfected with either the negative (sh-NC) or positive (sh-KLF8) control groups.

2.18 Chromatin Immunoprecipitation (ChIP)

H1299 and A549 cells were treated with 1% formaldehyde (Sigma-Aldrich) to cross-link DNA and proteins. Following this, the chromatin was sonicated to generate chromatin fragments using a Branson digital sonifier SFX 550 (Emerson, Danbury, CT, USA). Immunoprecipitation was carried out using anti-KLF8 (PA5-109885, 1:1000, Thermo Fisher Scientific), with a non-specific IgG (ab6715, 1:10,000, Abcam) used as the control. The immunoprecipitated DNA was purified and analyzed by qRT-PCR. Amplified PCR products were loaded on a 2% agarose gel with ethidium bromide and ImageJ2 software was used for quantitation. Relative enrichment of SIRT2 promoter fragment binding to anti-KLF8 or anti-IgG was calculated by comparing the ChIP signal intensity to the input DNA control [25]. The primer sequences used in the ChIP assays were as follows: SIRT2: Forward: 5′-CACCACATGGCTGTCTGTTT-3′; Reverse: 5′-TGGTGGAGGTGGCTAAATGT-3′.

2.19 Statistical Analysis

Data were processed using GraphPad Prism software (version 8.0.1, GraphPad Software Inc., San Diego, CA, USA) and presented as the mean ± standard deviation (SD). All experiments were conducted in triplicate. Student's *t*-test was used to analyze the statistical difference between 2 groups, while one-way ANOVA followed by Tukey's test was used for comparisons among three or more groups. Correlation was analyzed using Pearson's correlation coefficient. Each experiment was performed in triplicate. A *p*-value of less than 0.05 was considered statistically significant.

3. Results

3.1 KLF8 is Upregulated during Serum Starvation

The expression of KLF8 under serum starvation conditions was initially examined to investigate its role in nutrient deprivation. qRT-PCR, western blotting (WB) and immunohistochemistry (IHC) revealed upregulation of both relative KLF8 transcript and protein expression in LUAD tissues, when compared to normal controls (Fig. 1A–C). Additionally, qRT-PCR demonstrated higher KLF8 mRNA abundance in numerous LUAD cell lines, specifically, A549, H460, H1299, and HCC827, when compared to BEAS-2B normal cells (Fig. 1D). The expression of KLF8 in H3122 cells in serum-containing and serum starvation conditions was analyzed by GEO2R based on GSE62663 dataset, and the results revealed that KLF8 expression was significantly upregulated in LUAD cells under serum starvation conditions compared to control conditions (Fig. 1E). qRT-PCR and WB experiments also demonstrated higher KLF8 expression in LUAD cells under serum deprivation than under normal culture medium serum conditions (Fig. 1F–G).

3.2 KLF8 Maintains Cell Survival under Nutrient-Deprived Conditions

A previous study has reported that KLF8 promotes lung cancer cell growth and cell cycle progression in nor-

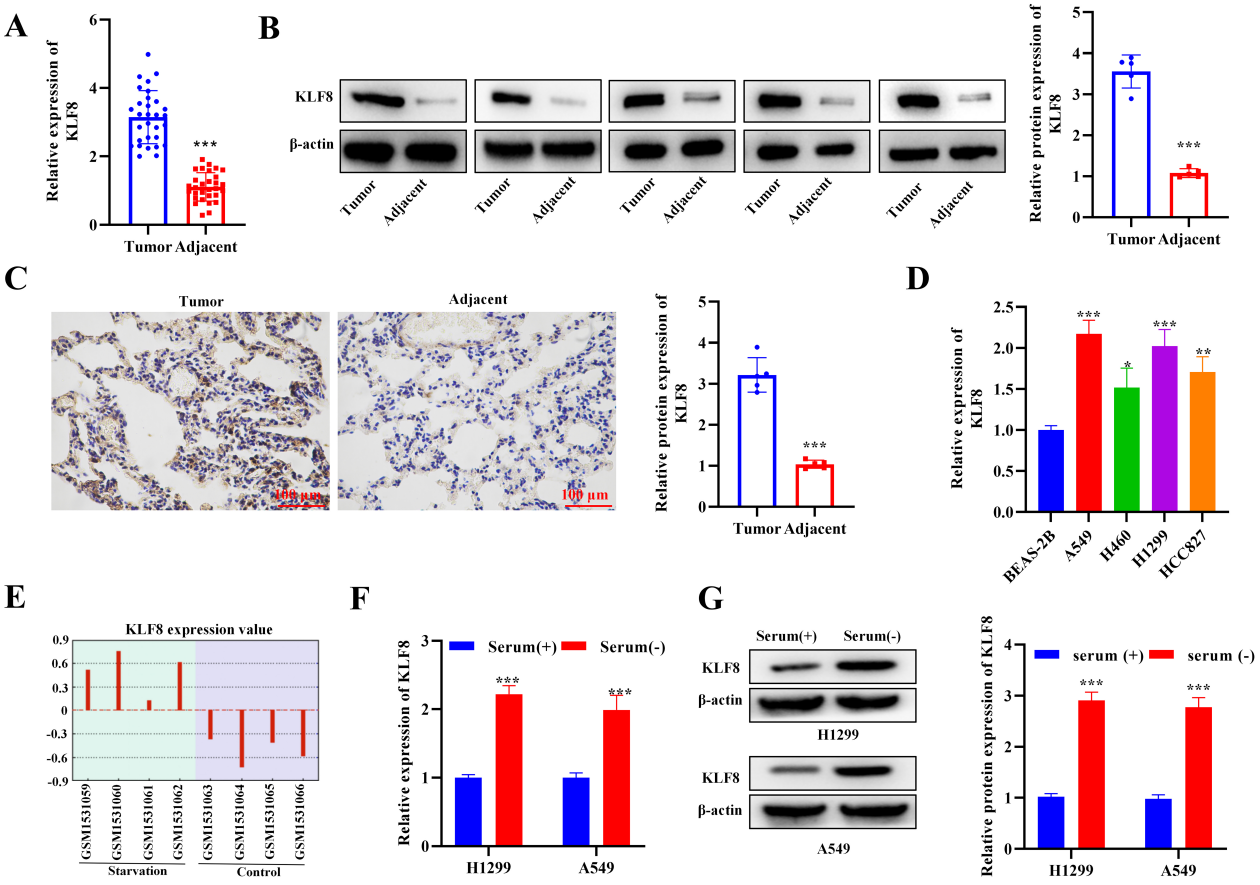

Fig. 1. Krüppel-like factor 8 (KLF8) is upregulated in lung adenocarcinoma (LUAD) tissues and serum starved LUAD cell lines. (A) Quantitative real-time polymerase chain reaction (qRT-PCR) was used to measure the expression of KLF8 in tumor tissues (n = 30) and adjacent normal tissues (n = 30). (B,C) KLF8 expression in normal/LUAD tissues (n = 5), detected via western blotting (WB) and immunohistochemistry (IHC). (D) KLF8 expression in normal/LUAD cells (A549, H460, H1299, HCC827) and human bronchial epithelial cells (BEAS-2B), detected via qRT-PCR. (E) KLF8 expression under starvation or control conditions, analyzed in the GSE62663 dataset using GEO2R. (F,G) Relative expression of KLF8, detected via qRT-PCR or WB, in H1299 and A549 cells grown in serum (+) or no serum (-) groups. $*p < 0.05$, $**p < 0.01$, $***p < 0.001$.

mal culture conditions [18]. Thus, we focused on the role of KLF8 in LUAD cell survival under nutrient-deprived conditions via overexpression and RNA interference experiments. Relative overexpression and interference efficiency are shown in Fig. 2A,B. CCK-8 assays showed that the LUAD cell viability was suppressed under serum starvation conditions compared with the serum-fed condition. Additionally, H1299 and A549 cell viability was relatively higher in the recombinant KLF8 serum-deprivation group relative to the Vector only serum-deprivation group, and further inhibited in the KLF8 knockdown (sh-KLF8 and serum-deprivation group relative to the shRNA control, serum-deprivation group (Fig. 2C,D). Colony formation assays revealed that overexpression of KLF8 increased the number of H1299 and A549 cell colonies in the KLF8 serum-deprivation group compared to the Vector serum-deprivation group, while KLF8 knockdown decreased colony formation in the KLF8-knockdown, serum (-) group compared to the control knockdown (sh-NC) serum-deprivation group (Fig. 2E,F). Flow cytometry indicated that KLF8 overexpression suppressed apoptosis in the KLF8 serum-deprivation group compared to the Vector control, serum (-) group, while KLF8 knockdown elevated apoptosis in the sh-KLF8 serum (-) group compared to the control sh-NC serum (-) group (Fig. 2G,H).

3.3 KLF8 Induced Increased Metabolism via PPP

It has been reported that under high ROS conditions, tumors can maintain cell proliferation by regulating metabolic reprogramming through PPP [26], and some studies have found that modulating PPP under cell starvation conditions contributes to cell survival [10]. We found that the ROS level was significantly increased in H1299 and A549 cells during nutrient deprivation (serum (-)) conditions compared with the control sh-NC serum (+) or Vector serum (+) groups. This was further enhanced by KLF8

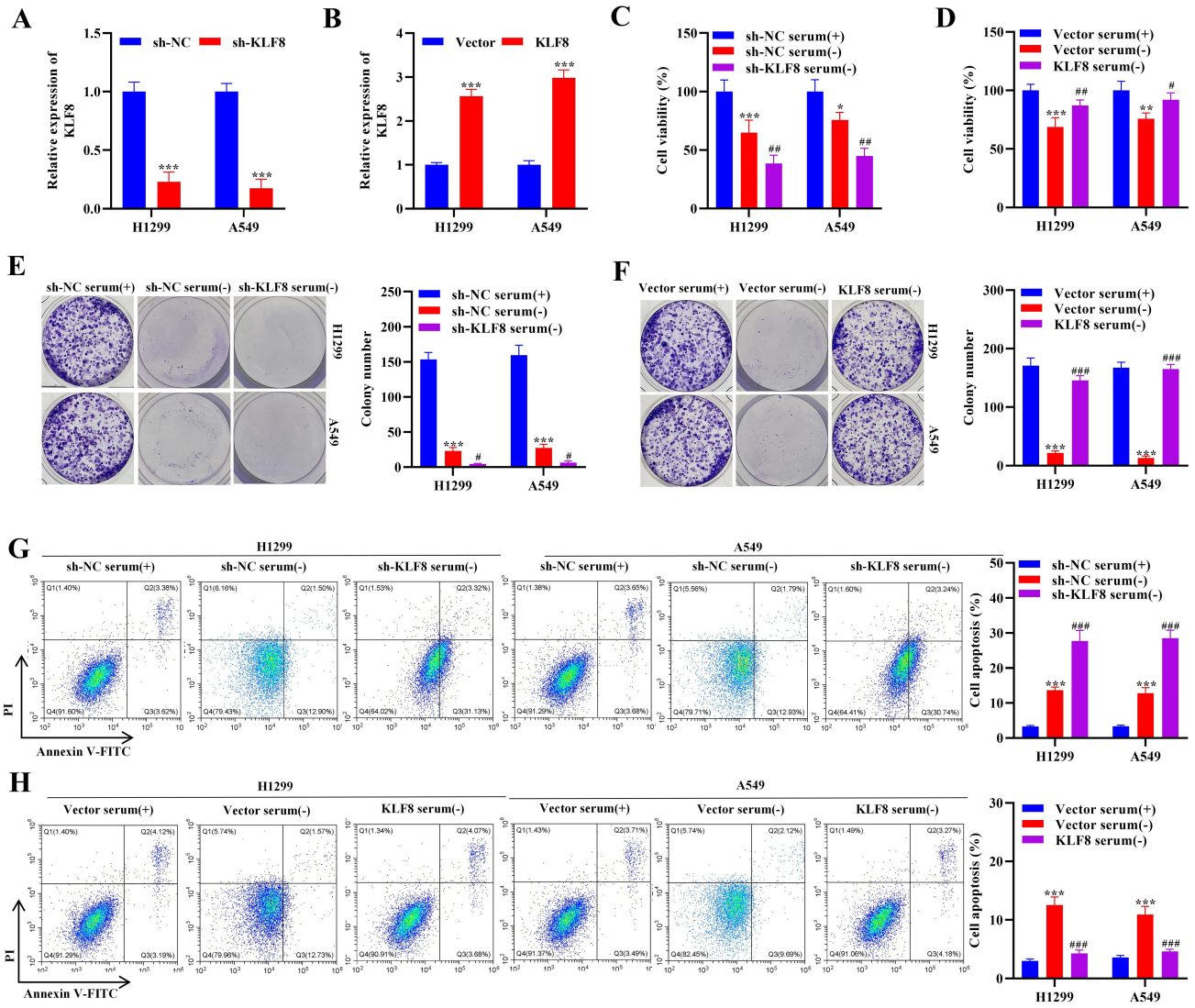

Fig. 2. KLF8 promoted the survival of H1299 and A549 cells under serum starvation conditions. (A,B) KLF8 overexpression and shRNA knockdown efficiency in H1299 and A549 under serum starvation conditions as assessed by qRT-PCR. ***$p < 0.001$ when compared to the control sh-NC vector group. (C,D) Cell viability of H1299 and A549 cells as assayed via cell counting kit-8 (CCK-8). (E,F) Cell growth of H1299 and A549 cells, assessed via colony formation assay. (G,H) Apoptosis of H1299 and A549 cells with KLF8 overexpression and knockdown and cultured in the presence or absence of serum was assessed via flow cytometry. *$p < 0.05$, **$p < 0.01$, ***$p < 0.001$ vs the serum control (+) group; $^{\#}p < 0.05$, $^{\#\#}p < 0.01$, $^{\#\#\#}p < 0.001$ vs the control sh-NC serum (-) or Vector serum (-) group.

knockdown and decreased by recombinant KLF8 overexpression. Moreover, overexpression or knockdown of KLF8 in serum (+) condition showed no significant impact on the ROS levels in H1299 and A549 cells (Fig. 3A,B).

We next explored whether KLF8 had an effect on PPP. KLF8 knockdown (Fig. 3C,E,G) resulted in significantly lower NADPH/$NADP^+$ ratios, decreased oxidate PPP flux, and lower RNA synthesis rates when compared to the control sh-NC/serum (-) group and the sh-NC serum (+) group. Levels were further elevated by KLF8 silencing in serum starvation conditions compared with the sh-NC serum (-) group. KLF8 overexpression (Fig. 3D,F,H) showed that compared with the Vector serum (+) group, the Vector serum (-) group had significantly higher NADPH/$NADP^+$ ratios, increased oxidate PPP flux, and higher RNA synthesis rates. Further, these levels were reduced by KLF8 overexpression in serum (-) conditions compared with Vector serum (-) group. Moreover, we also observed that KLF8 overexpression or knockdown in serum (+) conditions did not significantly change the NADPH/$NADP^+$ ratios, oxidate PPP flux and RNA synthesis rates compared with the control serum (+) groups. These results suggest that KLF8 activated the PPP and promoted increased metabolism in H1299 and A549 cells under starvation conditions.

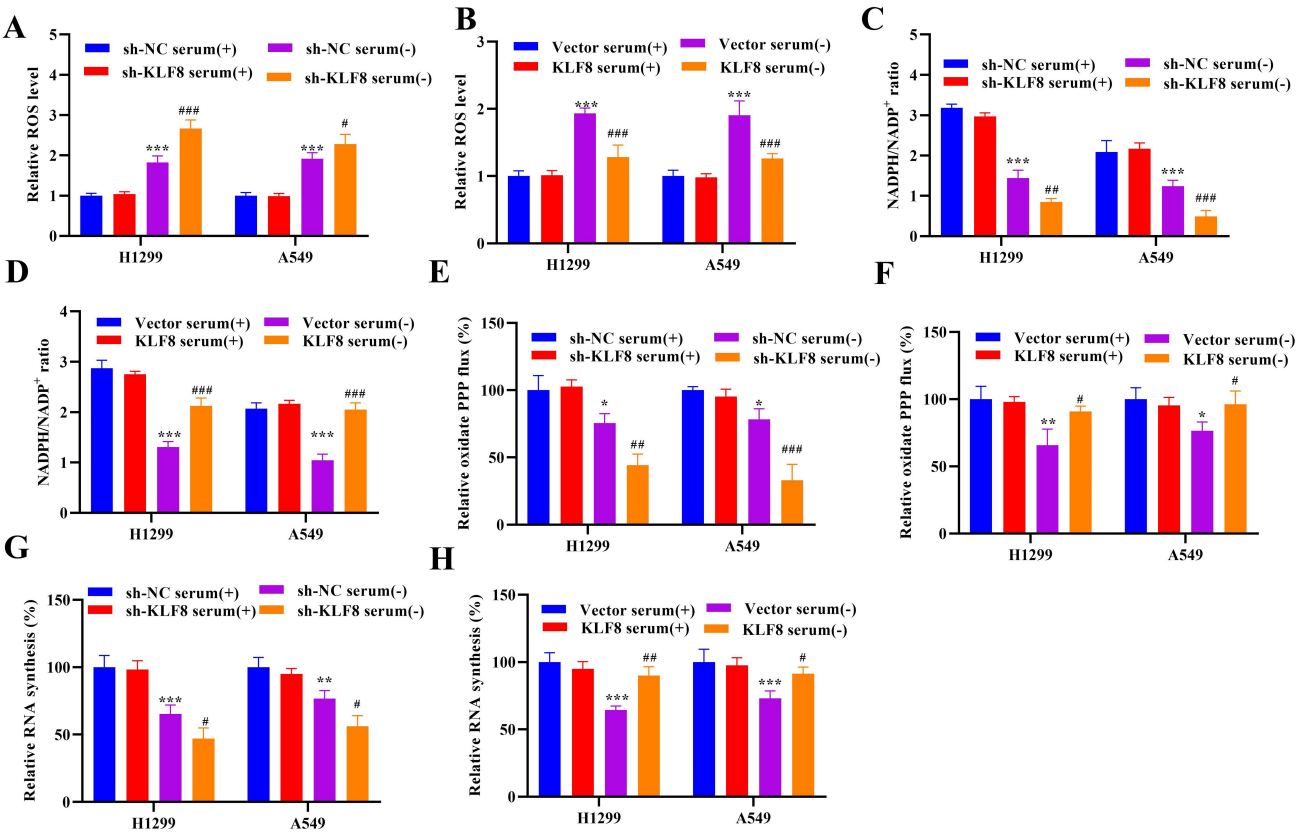

Fig. 3. KLF8 promoted the metabolism in H1299 and A549 cells via pentose phosphate pathway (PPP). (A,B) Relative reactive oxygen species (ROS) level in H1299 and A549 cells from sh-NC/KLF8 or Vector/KLF8 group and cultured under serum (+) or serum (-) conditions. (C,D) NADPH/$NADP^+$ ratio in H1299 and A549 cells from sh-NC/KLF8 or Vector/KLF8 group and cultured in serum (+) or serum (-) medium. (E,F) Relative oxidate PPP flux (%) in H1299 and A549 cells transfected with sh-NC/KLF8 or Vector/KLF8 and cultured in serum (+) or serum (-) medium. (G,H) The effects of KLF8 knockdown or overexpression on RNA biosynthesis rates in H1299 and A549 cells cultured in serum (+) or serum (-) medium. $^*p < 0.05$, $^{**}p < 0.01$, $^{***}p < 0.001$ vs the sh-NC/Vector serum (+) group; $^{\#}p < 0.05$, $^{\#\#}p < 0.01$, $^{\#\#\#}p < 0.001$ vs the sh-NC serum (-) or Vector serum (-) group.

3.4 KLF8 Enhances the Activity of G6PD

ShRNA-mediated knockdown of KLF8 significantly decreased G6PD activity in both H1299 and A549 cell lines compared to the sh-NC control group under both serum (+) and serum (-) conditions, and the overexpression of KLF8 had the opposite effect (Fig. 4A,B). However, qRT-PCR and western blotting confirmed that sh-KLF8 or KLF8 overexpression had no significant impact on G6PD expression at either the mRNA and protein levels in H1299 and A549 cells in both serum (+) and serum (-) conditions (Fig. 4C–F). In addition, LUAD patients with high G6PD expression exhibited poor overall survival ($p = 4.4 \times 10^{-7}$) (Fig. 4G). It has been reported that G6PD activity is affected by protein acetylation [27].

To better understand this effect, acetylation of the G6PD protein was investigated in H1299 and A549 cells transfected with sh-NC or sh-KLF8 using immunoprecipitation. Using anti-G6PD, pan-acetylation antibody detected increased lysine acetylation in the sh-KLF8 group under both serum (+) and serum (-) conditions. This finding demonstrated that KLF8 knockdown increased the acetylation of G6PD in both H1299 and A549 cells (Fig. 4H,I). Further, these findings suggested that KLF8 enhances G6PD activity through promoting G6PD post-translational modification rather than controlling transcriptional regulation during both serum (+) and serum (-) conditions.

3.5 KLF8 Regulated Serum Starvation-Induced Growth Inhibition through G6PD

To investigate whether G6PD mediated the effect of KLF8 on serum starvation-induced growth inhibition, H1299 and A549 cells were transfected with G6PD under serum (-) condition, overexpression efficiency is shown in Fig. 5A. As shown in Fig. 5B, overexpression of G6PD partially rescued the cell viability reduction caused by KLF8 knockdown in both H1299 and A549 cells under serum starvation. The colony formation assays further confirmed that G6PD overexpression partially reversed the inhibitory effect of sh-KLF8 on LUAD cell growth under serum (-) conditions (Fig. 5C). Moreover, flow cytometry analy-

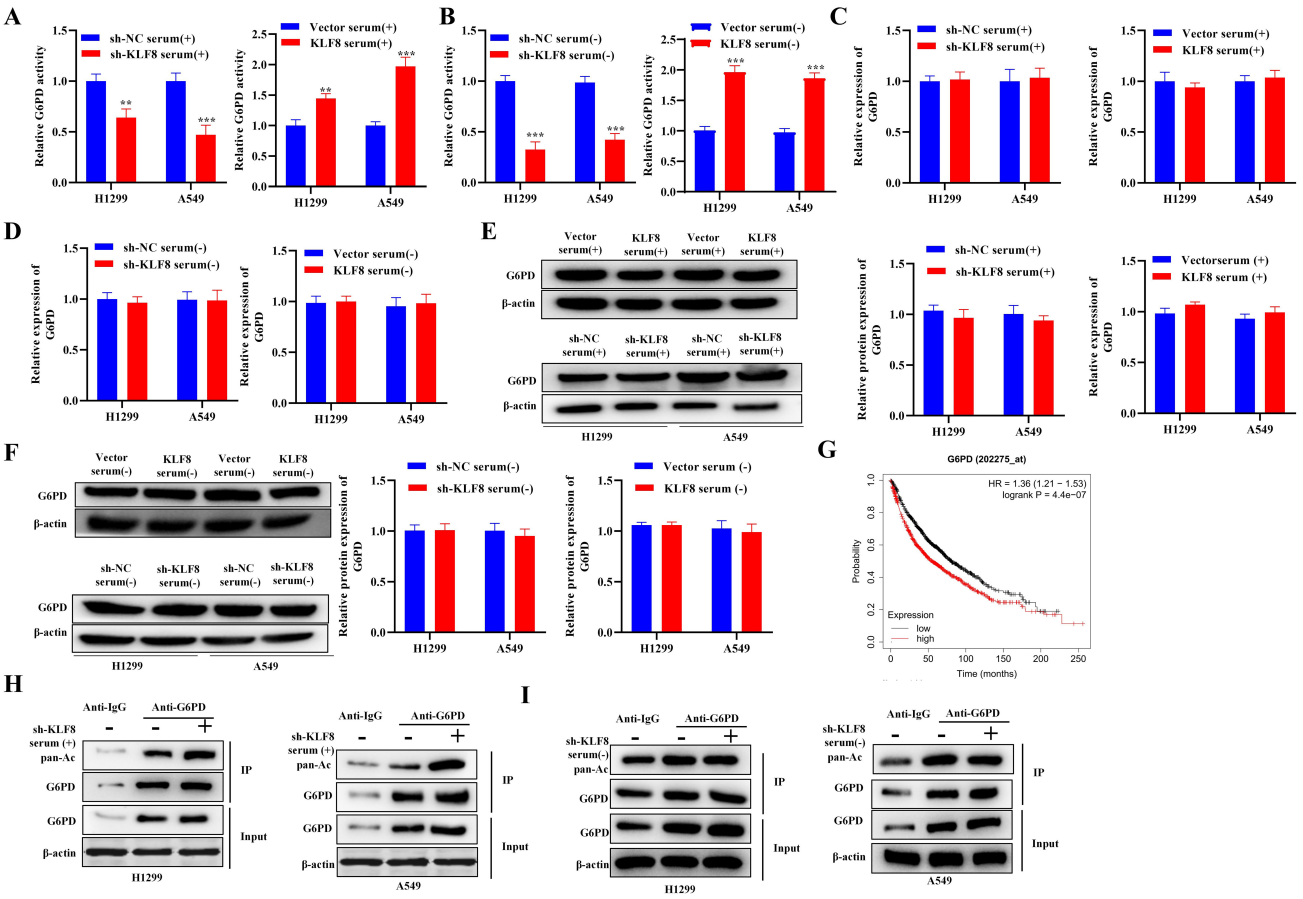

Fig. 4. KLF8 inhibits glucose-6-phosphate dehydrogenase (G6PD) acetylation to elevate G6PD protein activity. (A,B) Relative G6PD activity in H1299 and A549 cells under serum (+) and serum (-) conditions was measured in sh-NC or sh-KLF8 or Vector or KLF8-overexpression groups. (C–F) Relative G6PD expression in H1299 and A549 cells under serum (+) and serum (-) conditions in sh-NC or sh-KLF8 or Vector or KLF8-overexpression groups, assessed via qRT-PCR and WB. (G) Survival plot of LUAD patients with high or low G6PD expression using the Kaplan-Meier Plotter database. (H,I) Acetylation of G6PD in H1299 and A549 cells under serum (+) and serum (-) conditions from sh-NC and sh-KLF8 groups, assessed by immunoprecipitation/WB. $^{**}p < 0.01$, $^{***}p < 0.001$.

sis revealed that G6PD overexpression significantly decreased apoptosis rates induced by KLF8 knockdown in both cell lines under serum starvation conditions (Fig. 5D). Furthermore, G6PD overexpression also reversed the decrease of measured ROS levels (Fig. 5E), NADPH/NADP$^+$ ratio (Fig. 5F), oxidate PPP flux (Fig. 5G), and RNA synthesis (Fig. 5H) were each induced by KLF8 knockdown in H1299 and A549 cells during serum starvation. In addition, we also verified that KLF8 reversed the serum starvation-induced growth inhibition via G6PD using the G6PD inhibitor 6-aminonicotinamide (6-AN). As shown in Fig. 6A,B, the viability and proliferation of H1299 and A549 cells was elevated by KLF8 overexpression under serum (-) condition compared with the vector serum (-) group, and the 6-AN administration restored the basal level of proliferation. Moreover, apoptosis in H1299 and A549 cells was reduced by overexpressing KLF8 under serum (-) conditions relative to the Vector serum (-) group. Furthermore, 6-AN treatment rescued the impact that KLF8 overexpression exerted on LUAD cell apoptosis (Fig. 6C). Additionally, 6-AN treatment reversed ROS levels, NADPH/NADP$^+$ ratio, oxidate PPP flux, and RNA synthesis rate increased as a result of KLF8 overexpression in H1299 and A549 cells under serum (-) conditions (Fig. 6D–G). These results suggest that KLF8-regulated, serum starvation-induced, growth inhibition occurs through promoting G6PD-mediated PPP activity.

3.6 KLF8-Activated Transcription of SIRT2

Based on previous findings [20], KAT9 and SIRT2 are known to regulate G6PD acetylation. Gene Expression Profiling Interactive Analysis (GEPIA) analysis showed that KLF8 and SIRT2 were positively correlated in lung cancer tissues, and that there was no significant correlation between the expression of KLF8 and KAT9 (Fig. 7A). We next examined the effects of KLF8 knockdown or overexpression on the expression of KAT9 and SIRT2 using qRT-PCR and WB in A549 and H1299 cells transfected with sh-NC, sh-KLF8, empty Vector, or KLF8-expressing Vector. The results showed a positive correlation between SIRT2

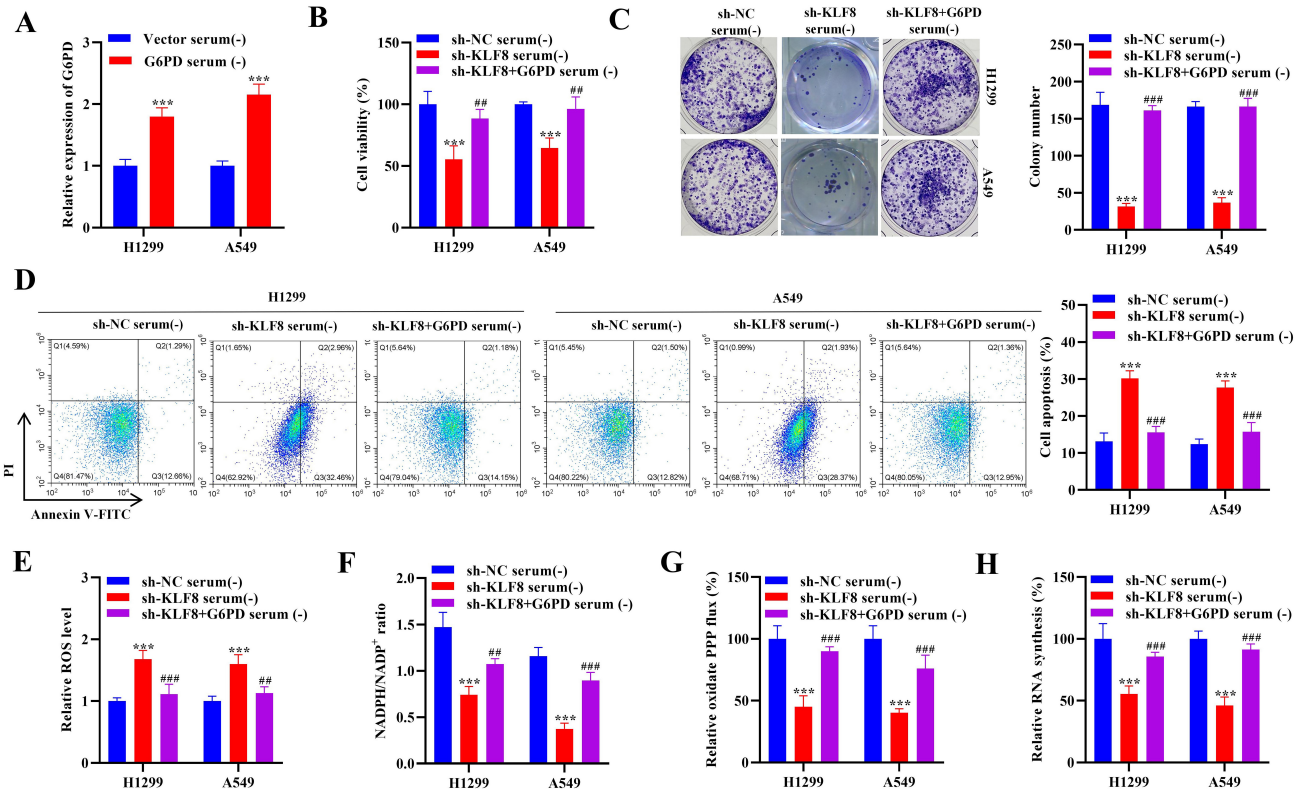

Fig. 5. KLF8 regulates the serum starvation-induced inhibition on cell growth via G6PD. (A) Overexpression of G6PD in H1299 and A549 cells as measured via qRT-PCR under serum (-) conditions. (B) Cell viability of H1299 and A549 cells under serum (-) conditions from sh-NC/sh-KLF8/sh-KLF8+G6PD group as assessed by CCK-8. (C) H1299 and A549 cell growth under serum (-) conditions from sh-NC/sh-KLF8/sh-KLF8+G6PD groups as assessed by colony formation assay. (D) Apoptosis of H1299 and A549 cells under serum (-) conditions from sh-NC/sh-KLF8/sh-KLF8+G6PD group as assessed by flow cytometry. (E) Relative ROS level in H1299 and A549 cells under serum (-) condition from sh-NC/sh-KLF8/sh-KLF8+G6PD group cells as assessed using fluorescent probes. (F) NADPH/$NADP^+$ ratio in H1299 and A549 cells under serum (-) condition from sh-NC/sh-KLF8/sh-KLF8+G6PD group cells as measured using a colorimetric assay. (G) Relative oxidate PPP flux (%) in H1299 and A549 cells under serum (-) condition from sh-NC/sh-KLF8/sh-KLF8+G6PD group cells. (H) Relative RNA synthesis rates under serum (-) conditions in H1299 and A549 cells from sh-NC/sh-KLF8/sh-KLF8+G6PD group cells. ***$p < 0.001$ when compared to the sh-NC serum (-) group; $^{\#\#}p < 0.01$, $^{\#\#\#}p < 0.001$ when compared to the sh-KLF8 serum (-) group.

and KLF8 expression (Fig. 7B–D). Moreover, the Kaplan-Meier Plotter website showed that LUAD patients with high SIRT2 expression had adverse survival outcomes (Fig. 7E).

Next, the binding sites for KLF8 on the *SIRT2* promoter was predicted using the HumanTFDB website (Fig. 7F). To confirm the results of this analysis, luciferase activity in H1299 and A549 cells showed a significant decrease after KLF8 knockdown in the group transfected with the promoter-WT probe. In contrast, findings showed no significant alteration in luciferase activity when cells were transfected with promoter-MUT. These findings indicate that KLF8 activates SIRT2 transcription (Fig. 7G). Finally, chromatin immunoprecipitation (ChIP) results indicated that the SIRT2 promoter showed higher enrichment after immunoprecipitation with anti-KLF8 compared with negative control anti-IgG. This result indicates that KLF8 directly interacts with the SIRT2 promoter (Fig. 7H) and suggest that KLF8 may promote H1299 and A549 cell growth and survival by activating SIRT2 transcription (Fig. 7I).

4. Discussion

The correlation between LUAD and nutrient deprivation has been well established, and previous studies have shown that the tumor microenvironment (TME) under nutrient deprivation, hypoxia, and/or acidosis significantly influences angiogenesis, as well as the presence of exhausted T cells and immunosuppressive myeloid cells in LUADs [28,29]. Nutrient deprivation is already used in the clinic as a cancer treatment strategy. For example, L-asparaginase treatment is effective on acute lymphoblastic leukemia by removing asparagine from the blood and has proven to be successful in nutrient dependency-targeting therapy [30]. Therefore, investigating the mechanisms underlying LUAD

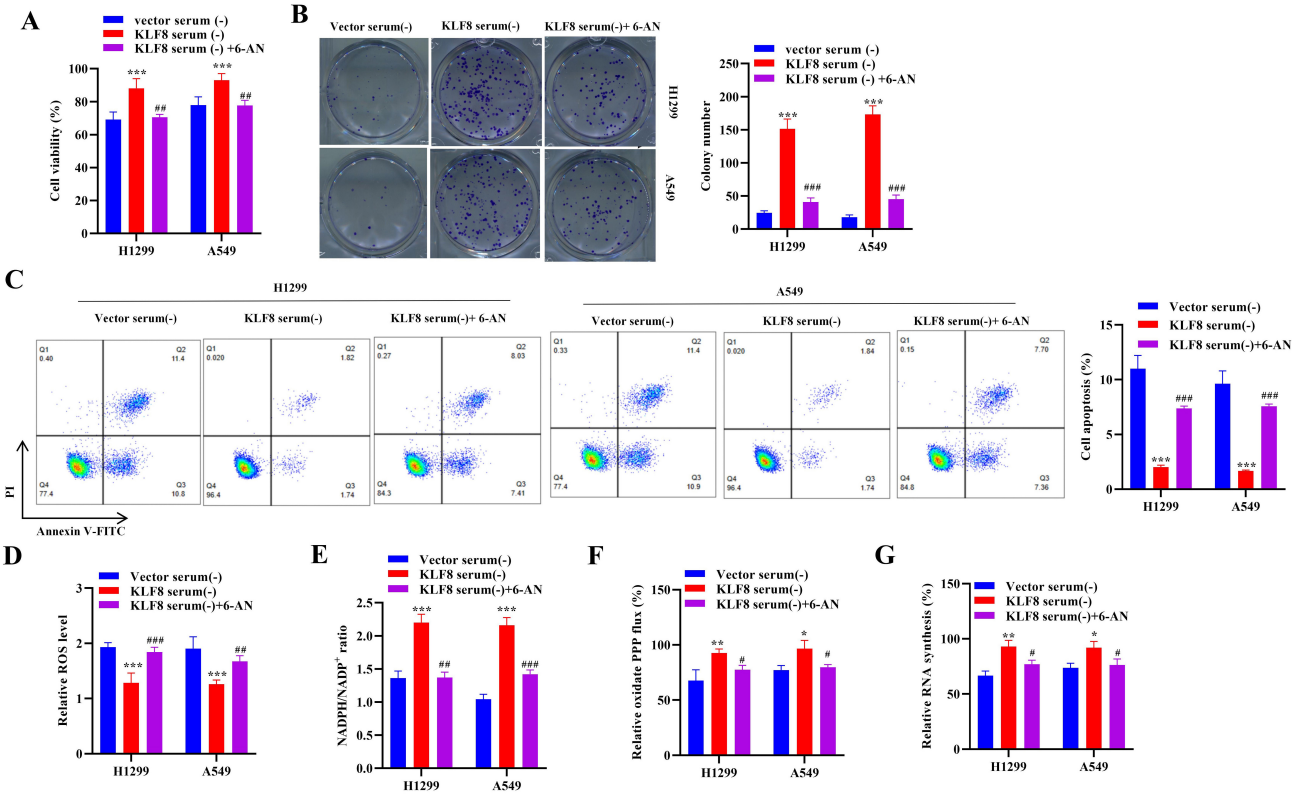

Fig. 6. The 6-AN treatment reversed the KLF8-induced enhancement on cell survival under serum starvation conditions. (A) Cell viability of H1299 and A549 cells under serum (-) conditions in the Vector/KLF8/and KLF8+6-AN group as measured by CCK-8 assay. (B) H1299 and A549 cell growth under serum (-) conditions in the Vector/KLF8/KLF8+6-AN groups as assessed by colony formation assay. (C) Apoptosis of H1299 and A549 cells under serum (-) conditions in Vector/KLF8/KLF8+6-AN group as measured by flow cytometry. (D) Relative ROS level in H1299 and A549 cells under serum (-) conditions in Vector/KLF8/KLF8+6-AN groups measured using fluorescent probes. (E) NADPH/$NADP^+$ ratio in H1299 and A549 cells under serum (-) conditions in Vector/KLF8/KLF8+6-AN groups measured using a colorimetric assay. (F) Relative oxidate PPP flux (%) in H1299 and A549 cells under serum (-) conditions in Vector/KLF8/KLF8+6-AN groups. (G) Relative RNA synthesis rate under serum (-) conditions in H1299 and A549 cells in Vector/KLF8/KLF8+6-AN groups. $^*p < 0.05$, $^{**}p < 0.01$, $^{***}p < 0.001$ when compared to the Vector serum (-) group; $^{\#}p < 0.05$, $^{\#\#}p < 0.01$, $^{\#\#\#}p < 0.001$ when compared to the KLF8 serum (-) group.

adaptation to nutrient-deprived conditions is of paramount importance, as this remains an understudied area in lung cancer research, with potentially significant implications for developing effective therapeutic strategies.

Relevant study by Li *et al.* [31] indicates that FOXA1 enhances LUAD cell survival in nutrient-deprived conditions by inhibiting autophagic cell death. Another study by Chen *et al.* [32] mentions that xanthine dehydrogenase, a rate-limiting enzyme in purine catabolism, plays a vital role in the survival of starved LUAD cells. Our study revealed the role of KLF8 under such conditions, and suggests KLF8 functions as a key regulator of the tumor immune microenvironment with a metastasis-promoting property in LUAD [33] during specific nutrient-deprived conditions. Our findings showed relative enhanced viability, colony number and apoptosis rate in KLF8 serum (-) group. The findings are in agreement with previous studies that showed increased KLF8 expression in various types of cancers, including lung cancer; however, our study further extends the understanding of KLF8 function in the adaptation of LUAD cells to nutrient deprivation.

While previous studies focused on the roles of specific regulator proteins, or enzymes, in promoting LUAD cell survival under nutrient deprivation, our study focused on understanding the regulation of PPP in this effect. Our work showed that KLF8 promoted oxidative PPP flux to facilitate PPP metabolism, and that this led to increased NADPH levels. This is consistent with previous studies that have shown that cancer cells rely heavily on the PPP to meet their metabolic demands [34,35].

In addition, our study provides a novel finding regarding the regulation of G6PD by acetylation. To our knowledge, this is the first study to show that KLF8 activates transcription of SIRT2 through suppression of G6PD acetylation. Acetylation is a type of post-translational modification that can regulate the activity of enzymes involved in various

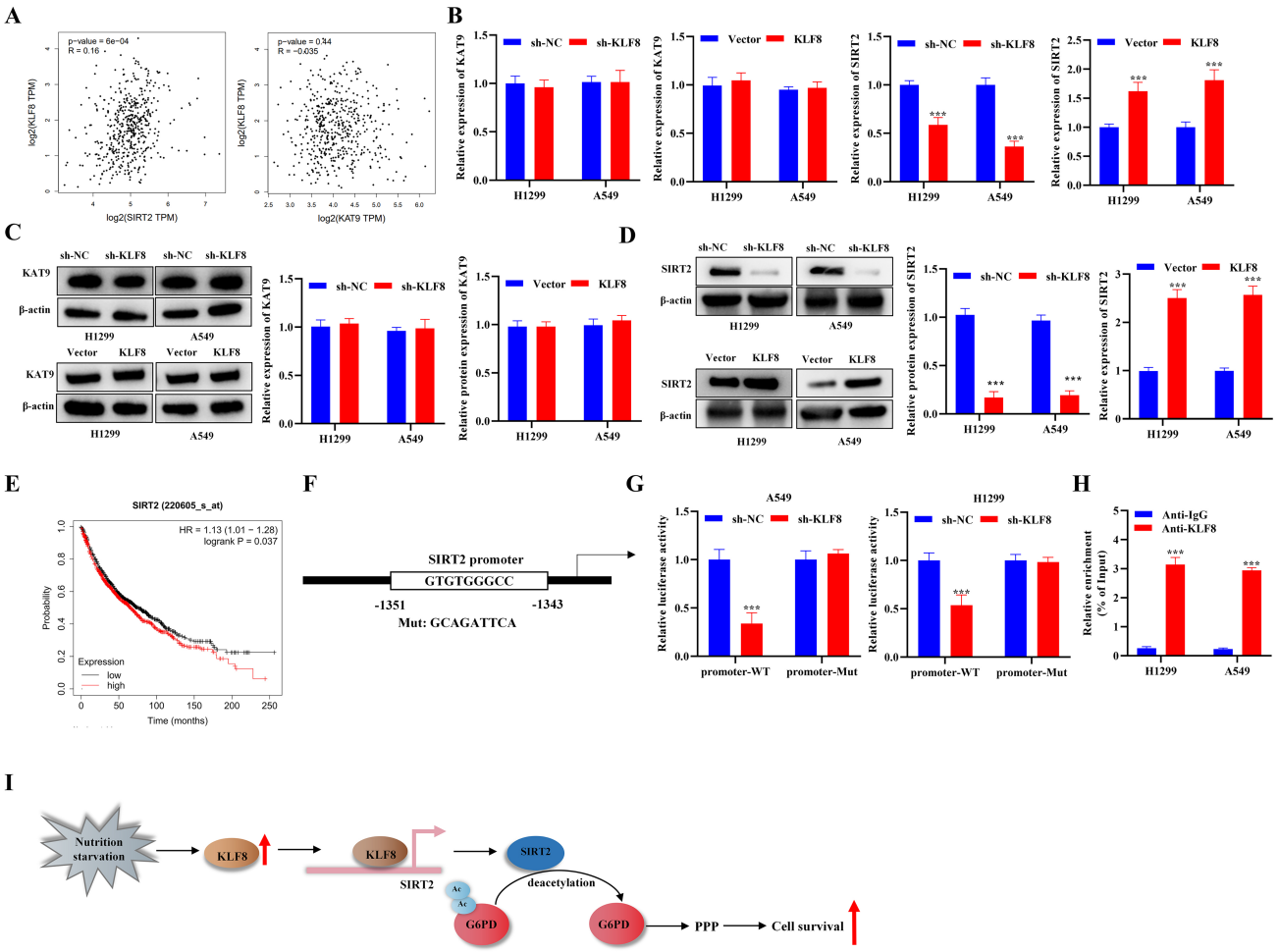

Fig. 7. KLF8 acted as a transcription factor of SIRT2. (A) Correlation between KLF8 and SIRT2, KLF8 and KAT9 was analyzed using Gene Expression Profiling Interactive Analysis (GEPIA). (B–D) Relative expression of KAT9 and SIRT2 in H1299 and A549 cells in the sh-NC/KLF8 or Vector/KLF8 group, detected by qRT-PCR and WB. (E) Survival plot of LUAD patients with high or low expression of SIRT2 on the Kaplan-Meier Plotter website. (F) Binding sites of KLF8 on SIRT2 promoters were predicted by the HumanTFDB website. (G) Relative luciferase activity in A549 and H1299 cells transfected with sh-NC/KLF8 and promoter-WT/Mut of SIRT2. (H) Relative enrichment (% of input) of SIRT2 promoter in the precipitates of anti-IgG/KLF8 in H1299 and A549 cells was detected using chromatin immunoprecipitation (ChIP) assays. (I) Graphical abstract of the study. ***$p < 0.001$.

metabolic pathways, including the PPP [36,37]. A previous study also indicates that SIRT2 suppresses the acetylation of G6PD [20]. G6PD catalyzes the first and rate-limiting step of the PPP, in which glucose-6-phosphate is converted into 6-phosphoglucono-δ-lactone with the concomitant production of NADPH. Under conditions of nutrient deprivation, cells may undergo metabolic reprogramming to adapt to the lack of nutrients. Aberrant activation of G6PD via metabolic reprogramming can alter NADPH levels, leading to either an antioxidant or a pro-oxidant environment as well as helping cells survive under conditions of nutrient deprivation [38]. This response may explain the mechanism underlying our findings.

There are still several limitations to our study. First, we focused on the role of KLF8-SIRT2-G6PD axis in lung adenocarcinoma under nutrient-deprived conditions but did not investigate other potential regulatory pathways involved in cancer metabolism. Second, our study did not investigate the potential of KLF8-SIRT2-G6PD axis as a therapeutic target *in vivo*. Further studies are needed to determine its potential as a target for lung adenocarcinoma therapy.

5. Conclusions

Our study provides new insights into the role of KLF8-SIRT2-G6PD axis in promoting the survival of LUAD under nutrient-deprived conditions. This work highlights the role of SIRT2 in regulating acetylation of G6PD, and could have implications for the development of new therapeutic strategies for this type of cancer.

Availability of Data and Materials

The datasets used and/or analyzed during the current study are available from the corresponding author on reasonable request.

Author Contributions

Conceptualization, QB and WJ. Methodology, QB, WJ and FC. Software, FZ. Validation, QB, WJ, and LL. Formal analysis, JZ and LC. Investigation, including cell culture, transfection, CCK-8, and colony formation assays, flow cytometry analysis, western blotting, PCR, immunoprecipitation, and Dual Luciferase Activity Reporter Assay, FC, JZ, and LC. Resources, FZ. Data curation, JZ, LC, YY, and FZ. Writing—original draft preparation, QB and WJ. Writing—review and editing, LL. Visualization, FC and JZ. Supervision, LL. Project administration, LL. All authors contributed to editorial changes in the manuscript. All authors read and approved the final manuscript. All authors have participated sufficiently in the work and agreed to be accountable for all aspects of the work.

Ethics Approval and Consent to Participate

The study was approved by the Ethics Committee of the Second Hospital of Nanjing has approved this study (2023-LY-kt085). Informed consent was obtained and signed by patients for all tissues.

Acknowledgment

Not applicable.

Funding

This research received no external funding.

Conflict of Interest

The authors declare no conflict of interest.

References

[1] Denisenko TV, Budkevich IN, Zhivotovsky B. Cell death-based treatment of lung adenocarcinoma. Cell Death & Disease. 2018; 9: 117.

[2] Huang L, Wang L, Hu X, Chen S, Tao Y, Su H, *et al*. Machine learning of serum metabolic patterns encodes early-stage lung adenocarcinoma. Nature Communications. 2020; 11: 3556.

[3] Bluemel G, Planque M, Madreiter-Sokolowski CT, Haitzmann T, Hrzenjak A, Graier WF, *et al*. PCK2 opposes mitochondrial respiration and maintains the redox balance in starved lung cancer cells. Free Radical Biology & Medicine. 2021; 176: 34–45.

[4] Patra KC, Hay N. The pentose phosphate pathway and cancer. Trends in Biochemical Sciences. 2014; 39: 347–354.

[5] Chen L, Zhang Z, Hoshino A, Zheng HD, Morley M, Arany Z, *et al*. NADPH production by the oxidative pentose-phosphate pathway supports folate metabolism. Nature Metabolism. 2019; 1: 404–415.

[6] Hayes JD, Dinkova-Kostova AT, Tew KD. Oxidative Stress in Cancer. Cancer Cell. 2020; 38: 167–197.

[7] Vultaggio-Poma V, Falzoni S, Chiozzi P, Sarti AC, Adinolfi E, Giuliani AL, *et al*. Extracellular ATP is increased by release of ATP-loaded microparticles triggered by nutrient deprivation. Theranostics. 2022; 12: 859–874.

[8] Pajak B, Siwiak E, Sołtyka M, Priebe A, Zieliński R, Fokt I, *et al*. 2-Deoxy-d-Glucose and Its Analogs: From Diagnostic to Therapeutic Agents. International Journal of Molecular Sciences. 2019; 21: 234.

[9] Ren Y, Shen HM. Critical role of AMPK in redox regulation under glucose starvation. Redox Biology. 2019; 25: 101154.

[10] Zhang Y, Xu L, Ren Z, Liu X, Song J, Zhang P, *et al*. LINC01615 maintains cell survival in adaptation to nutrient starvation through the pentose phosphate pathway and modulates chemosensitivity in colorectal cancer. Cellular and Molecular Life Sciences: CMLS. 2022; 80: 20.

[11] Tu D, Gao Y, Yang R, Guan T, Hong JS, Gao HM. The pentose phosphate pathway regulates chronic neuroinflammation and dopaminergic neurodegeneration. Journal of Neuroinflammation. 2019; 16: 255.

[12] Jeon SM, Chandel NS, Hay N. AMPK regulates NADPH homeostasis to promote tumour cell survival during energy stress. Nature. 2012; 485: 661–665.

[13] Thiepold AL, Lorenz NI, Foltyn M, Engel AL, Divé I, Urban H, *et al*. Mammalian target of rapamycin complex 1 activation sensitizes human glioma cells to hypoxia-induced cell death. Brain: a Journal of Neurology. 2017; 140: 2623–2638.

[14] Stanton RC. Glucose-6-phosphate dehydrogenase, NADPH, and cell survival. IUBMB Life. 2012; 64: 362–369.

[15] Cherukunnath A, Davargaon RS, Ashraf R, Kamdar U, Srivastava AK, Tripathi PP, *et al*. KLF8 is activated by TGF-β1 via Smad2 and contributes to ovarian cancer progression. Journal of Cellular Biochemistry. 2022; 123: 921–934.

[16] Kumar S, Behera A, Saha P, Kumar Srivastava A. The role of Krüppel-like factor 8 in cancer biology: Current research and its clinical relevance. Biochemical Pharmacology. 2021; 183: 114351.

[17] Zhao J, Bian ZC, Yee K, Chen BPC, Chien S, Guan JL. Identification of transcription factor KLF8 as a downstream target of focal adhesion kinase in its regulation of cyclin D1 and cell cycle progression. Molecular Cell. 2003; 11: 1503–1515.

[18] Ma D, Liu H, Qin Y, Tian Z, Li S, Liang N. KLF8 overexpression promotes the growth of human lung cancer cells by promoting the expression of JMJD2A. Cancer Cell International. 2019; 19: 258.

[19] Chamberlain KA, Huang N, Xie Y, LiCausi F, Li S, Li Y, *et al*. Oligodendrocytes enhance axonal energy metabolism by deacetylation of mitochondrial proteins through transcellular delivery of SIRT2. Neuron. 2021; 109: 3456–3472.e8.

[20] Wang YP, Zhou LS, Zhao YZ, Wang SW, Chen LL, Liu LX, *et al*. Regulation of G6PD acetylation by SIRT2 and KAT9 modulates NADPH homeostasis and cell survival during oxidative stress. The EMBO Journal. 2014; 33: 1304–1320.

[21] He J, Qiu N, Zhou X, Meng M, Liu Z, Li J, *et al*. Resveratrol analog, triacetylresveratrol, a potential immunomodulator of lung adenocarcinoma immunotherapy combination therapies. Frontiers in Oncology. 2023; 12: 1007653.

[22] Caffa I, D'Agostino V, Damonte P, Soncini D, Cea M, Monacelli F, *et al*. Fasting potentiates the anticancer activity of tyrosine kinase inhibitors by strengthening MAPK signaling inhibition. Oncotarget. 2015; 6: 11820–11832.

[23] Mao A, Zhou X, Liu Y, Ding J, Miao A, Pan G. KLF8 is associated with poor prognosis and regulates glycolysis by targeting GLUT4 in gastric cancer. Journal of Cellular and Molecular Medicine. 2019; 23: 5087–5097.

[24] Shan C, Lu Z, Li Z, Sheng H, Fan J, Qi Q, *et al*. 4-hydroxyphenylpyruvate dioxygenase promotes lung cancer growth via pentose phosphate pathway (PPP) flux mediated

by LKB1-AMPK/HDAC10/G6PD axis. Cell Death & Disease. 2019; 10: 525.
[25] Zhang Q, Shi R, Bai Y, Meng L, Hu J, Zhu H, *et al*. Meiotic nuclear divisions 1 (MND1) fuels cell cycle progression by activating a KLF6/E2F1 positive feedback loop in lung adenocarcinoma. Cancer Communications (London, England). 2021; 41: 492–510.
[26] Hyun DH. Insights into the New Cancer Therapy through Redox Homeostasis and Metabolic Shifts. Cancers. 2020; 12: 1822.
[27] Zhang X, Gao F, Ai H, Wang S, Song Z, Zheng L, *et al*. TSP50 promotes hepatocyte proliferation and tumour formation by activating glucose-6-phosphate dehydrogenase (G6PD). Cell Proliferation. 2021; 54: e13015.
[28] Osawa T, Shibuya M. Targeting cancer cells resistant to hypoxia and nutrient starvation to improve anti-angiogeneic therapy. Cell Cycle (Georgetown, Tex.). 2013; 12: 2519–2520.
[29] Li D, Yu H, Hu J, Li S, Yan Y, Li S, *et al*. Comparative profiling of single-cell transcriptome reveals heterogeneity of tumor microenvironment between solid and acinar lung adenocarcinoma. Journal of Translational Medicine. 2022; 20: 423.
[30] Tosta Pérez M, Herrera Belén L, Letelier P, Calle Y, Pessoa A, Farías JG. L-Asparaginase as the gold standard in the treatment of acute lymphoblastic leukemia: a comprehensive review. Medical Oncology (Northwood, London, England). 2023; 40: 150.
[31] Li J, Zhang Y, Wang L, Li M, Yang J, Chen P, *et al*. FOXA1 prevents nutrients deprivation induced autophagic cell death through inducing loss of imprinting of IGF2 in lung adenocarcinoma. Cell Death & Disease. 2022; 13: 711.
[32] Chen MM, Guo W, Chen SM, Guo XZ, Xu L, Ma XY, *et al*. Xanthine dehydrogenase rewires metabolism and the survival of nutrient deprived lung adenocarcinoma cells by facilitating UPR and autophagic degradation. International Journal of Biological Sciences. 2023; 19: 772–788.
[33] Jing P, Xie N, Zhao N, Zhu X, Li P, Gao G, *et al*. miR-24-3p/KLF8 Signaling Axis Contributes to LUAD Metastasis by Regulating EMT. Journal of Immunology Research. 2020; 2020: 4036047.
[34] Chen J, Fu Y, Hu J, He J. Hypoxia-related gene signature for predicting LUAD patients' prognosis and immune microenvironment. Cytokine. 2022; 152: 155820.
[35] Best SA, Ding S, Kersbergen A, Dong X, Song JY, Xie Y, *et al*. Distinct initiating events underpin the immune and metabolic heterogeneity of KRAS-mutant lung adenocarcinoma. Nature Communications. 2019; 10: 4190.
[36] Ding P, Ma Z, Liu D, Pan M, Li H, Feng Y, *et al*. Lysine Acetylation/Deacetylation Modification of Immune-Related Molecules in Cancer Immunotherapy. Frontiers in Immunology. 2022; 13: 865975.
[37] Guo P, Chen W, Li H, Li M, Li L. The Histone Acetylation Modifications of Breast Cancer and their Therapeutic Implications. Pathology Oncology Research: POR. 2018; 24: 807–813.
[38] Yang HC, Stern A, Chiu DTY. G6PD: A hub for metabolic reprogramming and redox signaling in cancer. Biomedical Journal. 2021; 44: 285–292.